Characterization and Application of New Apatitic Materials Synthesized from Hahotoé-Kpogamé Phosphate Rock

Dodji Zounon[1], Moursalou Koriko[1], Tomkouani Kodom[2*], Sanonka Tchegueni[1] and Gado Tchangbedji[1]

[1]Laboratoire Gestion Traitement et Valorisation des Déchets, Togo.
[2]Laboratoire d'Hydrologie Appliquée et Environnement, Togo.

Authors' contributions

This work was done in collaboration with all the authors. Author MK designed and supervised the study. The application of the synthesized materials was carried out under the supervision of author TK. He also contributed in the redaction and correction of the Manuscript. The interpretation of some results and the physico-chemical characterizations were carried out under author ST. Author GT as the director of the laboratory supervised all the work. All authors read and approved the final manuscript.

Original Research Article

ABSTRACT

Aims: Phosphorus and phosphate are broadly used in many areas ranging from advance researches to manufacturing companies for regular use purposes. In Togo, the raw phosphate is exploited and exported to serve as an ingredient in chemical fertilizers, detergents, phosphoric acid synthesis, etc. The aim of the present work is an investigation of alternative valuation of the raw phosphate of Hahotoé-Kpogamé in Togo.
Methodology: The study consists of the transformation of the raw phosphate into hydroxyapatite by dissolution followed by a precipitation. The hydroxyapatite thus obtained can be used, for example as a conditioning matrix of industrial waste, as a catalyst support, or for the depollution of water etc. The characterization was carried out by Fourier Transform Infrared Spectroscopy, X-Ray Diffraction,

_____

Corresponding author: E-mail: tchakodotom@yahoo.fr;

Thermogravimetric Analysis coupled to Thermal Differential Analysis and Inductively Coupled Plasma Atomic Emission Spectroscopy.

Results: These analyses revealed that the materials are predominantly of non-stoichiometric hydroxyapatite and minority of phosphate tricalcium and impurities. The synthesized materials (calcined and uncalcined) were applied as adsorbent and as coadsorbent of a photocatalyst (TiO2) for methylene blue removal. The study of the adsorption of the methylene blue was carried out in a batch mode. The adsorption of methylene blue on the synthesized materials gave a low yield (15 to 20%). However, used as in the mixture with titanium dioxide, the adsorption rate of methylen blue was increased significantly (57% of removal rate with 0.5 g synthesized materials + 2 g of TiO2 P25).

Conclusion: uncalcined hydroxyapatite obtained from raw phosphate can be used as an efficient co-adsorbent of titanium dioxide leading to an alternative valorization of this natural phosphate.

1. INTRODUCTION

Extraction and marketing of phosphate have started in Togo since 1957 [1,2]. The exploitation of this deposit is only intended for export after purification. The purified phosphates, once exported are used in the manufacturing industries of fertilizers and textile detergents etc.

On the agricultural level, phosphorus, contained in fertilizers, promotes the growth of the root system, regulates flowering and fruit ripening. Another area of the chemical phosphates industry is the production of fluorescent light tubes. Tons of fluorinated and chlorinated apatites obtained from the phosphate deposit and doped with magnesium and antimony are produced annually for this purpose. The phosphate extracted from the deposits is also used in the manufacture of foods, beverages, extinguisher powder, dental products in the treatment of the surface of metals, in the manufacture of matches, incendiary bombs, pyrotechnic products, in medicine, as well as in the tanning of leather and the refining of sugar [3]. Thus phosphates have many uses in everyday life. However, under certain conditions, they can get back up harmful to the environment. Phosphates in wastewater come largely from the agricultural activity, from domestic and industrial wastewaters. These phosphates, coupled with mineral nitrogen speeches in water, create the phenomena of eutrophication and dystrophication [4]. Indeed, not toxic in themselves for animal and plant life, they harm the environment when they are in high concentration. In fact, at high concentrations, phosphates contribute to excessively enrichment of aquatic environments with algae and macrophytes [2]. In order to reduce the amount of phosphate in wastewaters, the European Commission proposed, on November 4, 2010, to ban the use of phosphates in many manufactured products [4]. In view of this restriction on the use of phosphates, the long-term export of phosphate could pose socio-economic problems for the countries exporting the phosphate rock deposit such as Togo. It would then be necessary to look for alternative solutions, for example, transformation of natural phosphate into hydroxyapatite. Indeed hydroxyapatite has many interests in several areas. Much work has focused on the use of apatites, especially hydroxyapatites, for the removal of trace metallic elements from water [5–7].

Apatites are mineral compounds that are very stable thermally and chemically and have a high resistance to deterioration under radioactive radiation. Thus apatites can be effectively used as geological barriers in landfills, radioactive compounds storage centers etc [8–10]. Apatite can also be used as a good ion exchange barrier and as an adsorbent that is tested for dye removal and protein separation [11–17]. Apatite is also studied as a carrier for sustained-release drugs or as a catalyst support [15,18,19]. The objective of this study is to synthesize the hydroxyapatites from natural phosphates and then apply the characterized material to as adsorbents of methylene blue in water.

2. MATERIALS AND METHODS

2.1 Materials

2.1.1 Raw phosphate

This study was performed on the merchantable rock phosphate of Hahotoé-Kpogamé (TOGO). Commercial rock phosphate is obtained from this raw material after pretreatment.

Fig. 1. Commercial Phosphate of Hahotoé-Kpogamé (TOGO)

2.1.2 Hydroxyapatite obtained from natural rock phosphate

Fig. 2 shows hydroxyapatite obtained from phosphate rock after drying in an oven at 100°C and heating treatment in the oven at 1200°C. The heating changes the color from white to yellow.

2.1.3 Methylene blue as model pollutant

For application as adsorbent of new material synthesized, methylene blue (BM) or tetramethylthionine hydrochloride was used as model pollutant in water. It is a cationic dye of CI 52015 index with chemical formula $C_{16}H_{18}N_3SCl$
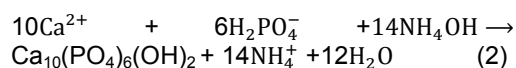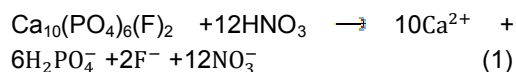
and molar mass about 319.85 gmol^{-1}. MB is an organic dye belonging to the Xanthines family.

2.1.4 TiO$_2$ as heterogeneous photocatalyst

Titanium dioxide (TiO$_2$) P25 from DEGUSSA is one of the photocatalysts regularly used as a reference in many studies related to organic removal by photocatalysis [20]. As a powder, the efficiency is very good compared to the same material fixed in the form of a thin layer [21]. In this study, TiO$_2$ was mixed with synthesized hydroxyapatite to increase specific area available for organics adsorption.

2.2 Synthesis of Hydroxyapatite from Phosphate Rock

The principle of this synthesis is based on the reaction of dissolution of natural phosphate in nitric acid (HNO$_3$) to release specifically the ions Ca^{2+} and PO_4^{3-} (eq. 1). After total dissolution of the natural phosphate, the mixture obtained is filtered [22]. The filtrate obtained is precipitated with a concentrated ammonia solution (eq. 2) [23]. The precipitate is then washed and dried:

$$Ca_{10}(PO_4)_6(F)_2 + 12HNO_3 \longrightarrow 10Ca^{2+} + 6H_2PO_4^- + 2F^- + 12NO_3^- \quad (1)$$

$$10Ca^{2+} + 6H_2PO_4^- + 14NH_4OH \longrightarrow Ca_{10}(PO_4)_6(OH)_2 + 14NH_4^+ + 12H_2O \quad (2)$$

Fig. 2. Uncalcined and calcined apatitic materials obtained from raw phosphate modification
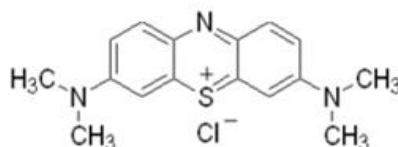

Fig. 3. Structure of methylene blue

3

The hydroxy apatitic material synthesized was calcined at 1200°C using a SNOL brand oven. The calcination was done in two steps:

- First step: the temperature was increased from ambient temperature to 1200°C with a gradient of 5°C / min.
- Second step: the temperature was then maintained at 1200°C for 2 hours.

2.2.1 Characterization of the synthesized materials

The materials were characterized at the Center for Analysis and Characterization (CAC) in Morocco.

Inductively Plasma Atomic Emission Spectrometry (ICP-AES) was used to determine the chemical composition. X-ray diffraction analysis (XRD) was performed to identify the crystallographic structures of the materials. Fourier Transform Infrared Spectroscopy (FTIR) was performed to determine the functional groups. Thermogravimetric analysis (TGA) and differential thermal analysis (DTA) were performed to determine the thermal behavior of the materials [24–27].

2.2.2 Adsorption experiment

The experiments were performed in "batch mode". In four Erlenmeyer flasks each containing 200 ml of dye solution numbered from 1 to 4, the masses m_1 = 2 g of TiO_2, m_2 = 2 g of TiO_2 + 0.5 g of the synthesized product, m_3 = 2 g of TiO_2, + 1 g of the synthesized product and m4 = 2 g of the synthesized product only. The synthesized material here corresponds to the raw material obtained after heat treatment at 105°C. The dye solutions were prepared by dissolving the required amounts of the dye in distilled water to obtain a concentration of 6.25×10^{-6} mol/L, i.e a concentration of 2 mg/L. The mixtures obtained were homogenized using a CIMAREC i multipoint magnetic stirrer at a speed of 800 rpm at room temperature. After each 30 min, for 3 h, 10 mL of the mixture is taken from each Erlenmeyer flask, centrifuged, and filtered to obtain a clear liquid for residual dye analysis on JENWAY brand UV-VIS 6705 spectrophotometer at 663 nm. The same experiments were repeated with materials calcined at 1200°C.

3. RESULTS AND DISCUSSION

The chemical and mineralogical compositions as well as the results of the application of the synthesized materials are presented and commented in this part.

3.1 Chemical Analysis

Elemental analysis (Table 1) performed using an ICP-AES spectrometer reveals the presence of calcium (Ca) and phosphorus (P) as major elements [28]. The analysis also reveals the presence of metallic trace elements in the synthesized materials.

Table 1. Elemental analysis

	Uncalcined product	Calcined product 1200°C
SiO_2 (%)	1,81	0,89
Al_2O_3 (%)	0,61	< 0,10
Fe_2O_3 (%)	0,94	0,74
CaO (%)	50,56	53,54
MnO (%)	0,04	0,03
P_2O_5 (%)	34,67	37,56
As (ppm)	99	96
Cu (ppm)	109	84
Ni (ppm)	70	65
Sr (ppm)	440	240
Zn (ppm)	217	194

From the data in Table 1, the Ca/P atomic ratio of each of the materials was calculated. The Ca/P atomic ratios of the calcined and uncalcined materials were 1.81 and 1.85, respectively. These values are higher than that of a stoichiometric phosphocalcic apatite (Ca/P = 1.67) [17]. This could be related to the presence of carbonates and other impurities, detected by infrared spectroscopy and thermal analysis, in materials. Indeed, there are two types of substitution by carbonates. The substitution of type A which concerns the ions OH^- and the second of type B which involves the ions PO_4^{3-}. Substitution of type B reduces the amount of phosphorus in the material, which has the effect of increasing the Ca/P atomic ratio of the materials. Heughebaert et al. have demonstrated a preferential localization of ions CO_3^{2-} in B sites when studying the influence of carbonate ions on the hydrolysis of precipitated calcium orthophosphates [29]. The increase in the Ca/P atomic ratio in this study could then be justified by substitution of type B.

3.2 X - Ray Diffraction of Synthesized Materials

The X-ray spectrum of the materials synthesized and dried at 105°C (Fig. 4) exhibits wide and

diffuse lines at room temperature, corresponding to a poorly crystallized product. After heat treatment at 1200°C, the materials diffractogram exhibits fine lines showing good crystallinity. According to PDF-2 file, the diffractogram correspond to two distinct phases, identified as hydroxyapatite and tricalcium phosphate β.

The first phase of the calcined products is identified with the hydroxyapatite referenced to the code 00 034 0010 of chemical formula $Ca_{10}(PO_4)_6(OH)_2$ crystallized in the hexagonal system, belonging to the space group $P6_3/m$ of parameters of mesh a = b = 9.4148 Å and c = 6.8791 Å [28]. The second phase is identified with tricalcium phosphate referenced to code 00 001 0941 of chemical formula $Ca_3(PO_4)_2$ [24].

3.3 Characterization of Materials by Fourier Transform Infrared Spectroscopy

Infrared spectroscopic analysis of the materials reveals several absorption bands (Fig. 5) which are listed in Table 2.

The analysis of the infrared spectra of the hydroxyapatites still has certain characteristic bands attributable to the phosphate ions (PO_4^{3-}) and the hydroxide ions (OH^-). In the spectrum of the non-calcined synthesized product (Fig. 5) a broad band between 3700 and 2700 cm^{-1} and another centered at 1640 cm^{-1} correspond to vibrations of elongation and deformation of the O-H bonds of the water molecules adsorbed by the material [28]. The bands around 3400 cm^{-1} and 1640 cm^{-1}, respectively, can be attributed to vibrations of elongation and deformation of the N

-H bonds of ammonia from synthetic reagents [27]. In addition, the same bands between 3700 and 3500 cm^{-1} could overlap the hydroxide ion elongation band (OH^-) which is often around 3560 cm^{-1}. But further, we find a shoulder at 632 cm^{-1} which corresponds to the vibrations of hydroxide ions (OH^-) [27,30].

The spectrum also shows an intense band centered at 1388 cm^{-1} and a peak at 825 cm^{-1} that can be attributed to carbonate ions [27]. Another small band around 2360 cm^{-1} can be attributed to adsorbed carbon gases at the surface of the product [27]. The spectrum logically shows characteristic bands of the phosphate ions. In fact, the bands at 1101 cm^{-1}, 1040 cm^{-1} and 964 cm^{-1} attributable to elongation vibrations of phosphate ions (PO_4^{3-}) are detected. Bands at 603 cm^{-1}, 574 cm^{-1} and 470 cm^{-1} always correspond to strain rates of the phosphate ions (PO_4^{3-}) [28]. After the heat treatment at 1200 °C of the synthesized product, we notice in the spectrum the disappearance of some bands (Fig. 5). The partial disappearance of the bands around 3180 cm^{-1} and the band at 1641 cm^{-1} shows the dehydration of the synthesized material by heat treatment. However, the presence of small bands around 3421 cm^{-1} and 1641 cm^{-1} can be explained by the existence of structural water molecules in the materials even after heat treatment. The peaks observed at 3541 cm^{-1} and 630 cm^{-1} on the spectrum after the heat treatment are assimilated to the frequency of elongation and vibration of the hydroxide ions (OH^-). But one can also notice that the peaks are not very intense and that there has been a shift of frequency of elongation because this peak is normally around

Table 2. Attribution of FTIR spectrum bands for materials

v (cm^{-1})	Uncalcined product	Calcined product 1200°C	References
3700-2700	H_2O/NH_3	H_2O	[27,28]
3560-3541	HO^-	HO^-	[27,30]
2360	CO_2	----	[27]
1640-1616	H_2O/NH_3	H_2O	[27,28]
1456-1388	CO_3^{2-}	----	[27,30]
1101-1098	PO_4^{3-}	PO_4^{3-}	[27]
1040	PO_4^{3-}/SiO_2	PO_4^{3-}/SiO_2	[27]
970	----	----	[27]
964	PO_4^{3-}	PO_4^{3-}	[27]
870-825	CO_3^{2-}	----	[27,30]
632-630	HO^-	HO^-	[27,30]
603-570	PO_4^{3-}	PO_4^{3-}	[27]
470	PO_4^{3-}/SiO_2	PO_4^{3-}/SiO_2	[27]

3560 cm^{-1}. The decrease in the intensity of these peaks can be explained by the substitution of the ions OH^- by the ions CO_3^{2-}. We also observe the disappearance of the bands located towards 1388 cm^{-1} and the peak at 825 cm^{-1}, which is explained by the decomposition of carbonate residues.

3.4 Thermal Analysis of Materials

Fig. 6 shows thermograms of thermogravimetric analysis coupled with differential thermal analysis

of materials. The curve of thermogravimetric analysis of materials (Fig. 6) shows mass losses in three temperature ranges. The first mass loss corresponding to 8.539% of the total mass of the sample occurred between room temperature and 157°C. This loss of mass is attributed to the physical desorption of water on the surface of the material. It can also be attributed to the decomposition of some organic matter that is little related to the apatite structure. The second loss of mass is the most important. It corresponds to 17.4% of the total mass and is
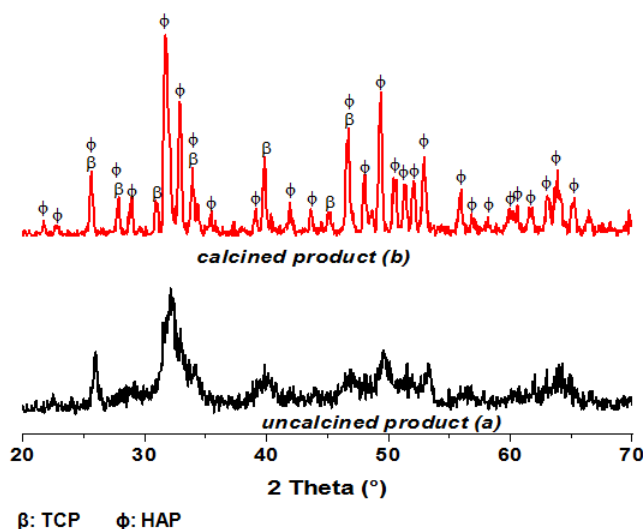

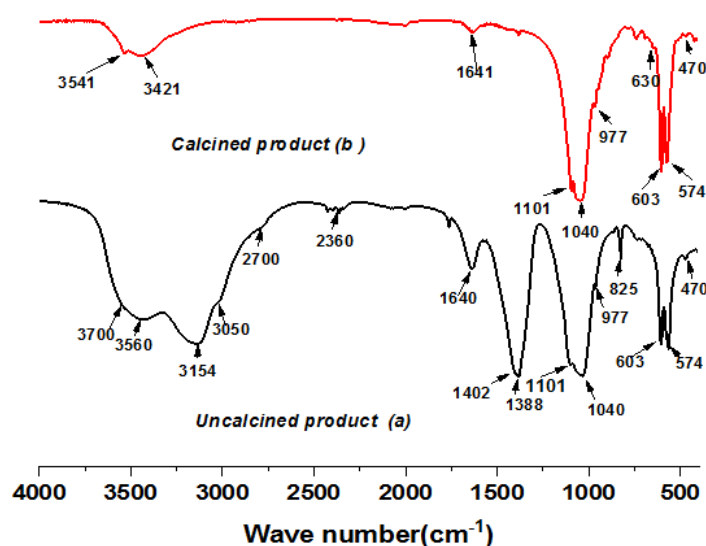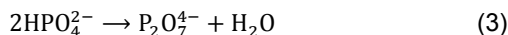**Fig. 4. X-ray diffraction patterns of uncalcined and calcined products**

Fig. 5. Infrared spectrograms of calcined and uncalcined products

detected between 165 and 294°C. This loss can correspond to the decomposition of a part of the organic matter and also to the desorption of the adsorbed water in the materials (eq.3).

$$2HPO_4^{2-} \longrightarrow P_2O_7^{4-} + H_2O \qquad (3)$$

The last loss of mass about 5.66% observed between 305 and 1017 °C is attributed to both the structural water dehydration and the decomposition of carbonates. This analysis is in agreement with interpretations made at the IR spectroscopy concerning the bands corresponding to water molecules adsorbed on the surface and in structures and carbonates.

The dehydration of the hydroxyapatite gives the non-stoichiometric hydroxyapatite according to the following chemical equation (eq. 4).

$$Ca_{10}(PO_4)_6(OH)_2 \rightarrow Ca_{10}(PO_4)_6(OH)_{2-2y}O_y + yH_2O \qquad (4)$$
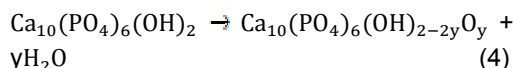
The Differential thermal Analysis (DTA) shows two exothermic peaks at 166°C and 279°C corresponding to exothermic decomposition of organic matter [31]. It is deduced that the DTA confirms the first losses reported by the TGA.

3.5 Application of Synthesized Materials as Adsorbents for Methylene Blue Removal

Fig. 7 shows the methylene blue removal rates with initial concentration of 2 mg/L, at pH = 7.6 at room temperature, using calcined and non-calcined synthesized materials (mass m = 2 g).

Two steps of adsorption could be noted: the first during the first thirty minutes corresponding to fast mechanism and a second slower. After 3 hours of contact with the adsorbents, the removal rates of about 20% are observed with the uncalcined materials and 15 % with the calcined products. These low adsorption rates can have several explanations like poor structuring and the presence of impurities resulting in a small surface area available for adsorption [25,32]. Indeed, infrared spectroscopic and thermal analysis of the synthesized materials have shown that it contains a significant amount of water and organic matter that might cause the clogging of macropores. As the consequence, the adsorption capacity of the materials will be small since the fluid access to the internal surface of the adsorbent is not significant. The low adsorption rates could be also due to an aggregation of the apatitic.

High thermal analysis could also lead to adsorption sites destruction explaining the poor adsorption capacity of annealing material.

To increase the adsorption rate of methylene blue, of synthesized materials, dispersion on titanium dioxide was performed.

The analysis of the removal rates in the case of the adsorbents represented by the mixtures of 2 g of TiO_2 with 0.5 g and 1 g respectively of the non-calcined synthesized material shows that the adsorption was carried out in two phases (Fig. 8). The first phase is fast with a 40% removal rate after 30 min. On the other hand, the second
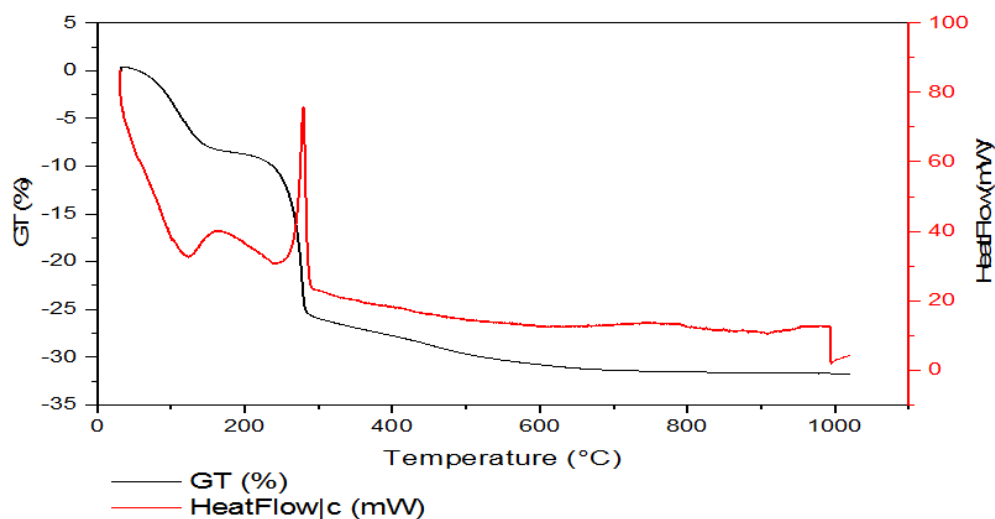

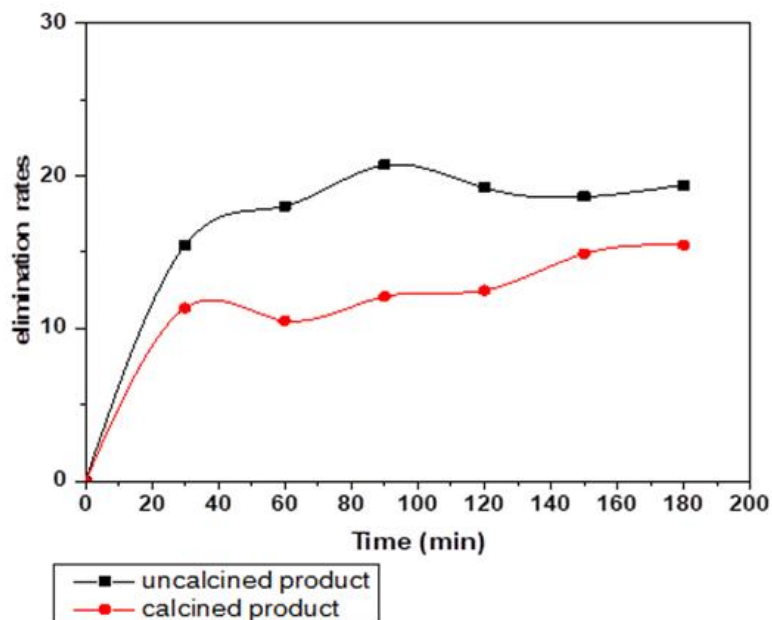**Fig. 6. TGA and DTA thermograms of the developed product**

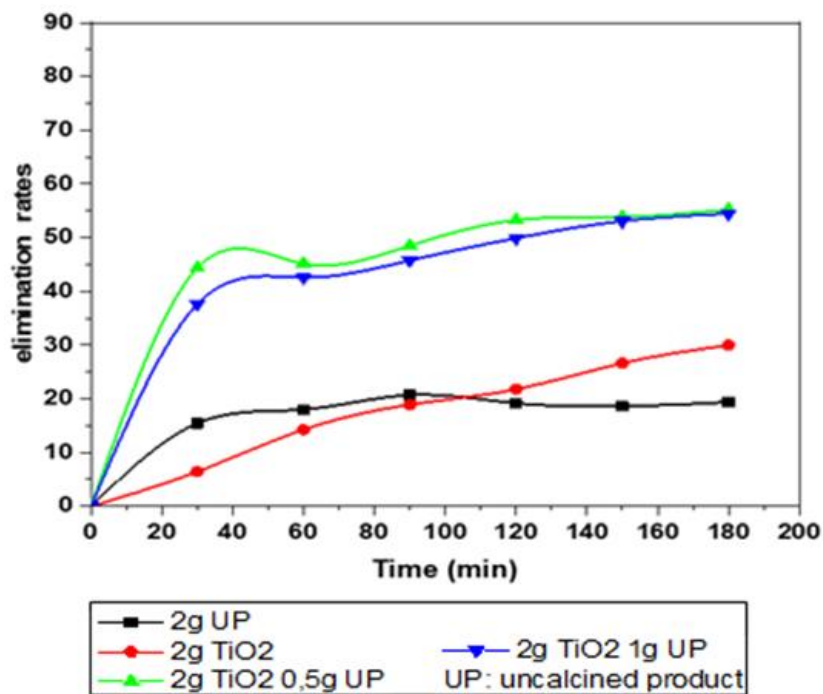**Fig. 7. Dye removal rate by calcined and uncalcined materials**

Fig. 8. Dye removal rate by TiO$_2$ mixed with the uncalcined apatite

phase is slow. After 3 hours as contact time, the removal rates was respectively of 57% and 56% for 2 g TiO$_2$ + 0,5 g of hydroxyapatite and TiO$_2$ + 1g of hydroxyapatite. This significant increase of adsorption rate could be resulted to synergetic effect of the two materials but also due to the dispersion of hydroxyapatite onto titanium dioxide.

Fig. 9. The solution of dye in the mixture after the adsorption study

It is also noted that the removal rate of the mixture containing 0.5 g of synthesized apatite is slightly greater than that containing 1 g of synthesized apatite. This phenomenon can be explained by the screen effect produced by the excess of the synthesized apatite. There would then be an optimum mass of apatite for which the synergistic effect with TiO_2 would be greater. Beyond this optimum mass, a proportion of nanoparticles of the TiO_2 photocatalyst will no longer be exposed for adsorption [33,34].

It was also noted that the mixture increases the settling rate after stopping the shaking. This mixture is a potential alternative to overcome the formation of the colloidal solution when using TiO_2 during photocatalytic studies. Indeed, TiO_2 is the most prominent material among photcatalysts. However, it uses in slurry form create a supplementary difficult due to the separation at the end of the photodegradation studies. It is thus possible to dispense with the very expensive step of nanofiltration in the case of the use of nanoparticles of TiO_2 [35–37] by using apatites as co-adsorbent for titanium dioxide. The apatite as co-adsorbent will also increase the adsorption rate of the pollutant since the adsorption is the determinative for direct photodegradation of the organic pollutant onto the TiO_2.

4. CONCLUSION

This study aims at contributing to an alternative valorization of the natural phosphate of Togo by a transformation of the natural phosphate into hydroxyapatite. For this purpose, new apatitic materials have been synthesized from Hahotoé-Kpogamé natural phosphate by dissolution followed by precipitation. The synthesized materials have been characterized by ICP, FTIR, XRD and thermals analysis. Chemical analysis revealed that the synthesized materials are constituted mainly of calcium and phosphate and some traces of iron, silicon, copper, aluminum, nickel, zinc, strontium and arsenic. Fourier Transform Infrared Spectroscopy revealed the presence of hydroxide ions (OH^-), phosphate ions (PO_4^{3-}) and carbonate ions (CO_3^{2-}) in the materials. The XRD diffractogramme of the synthesized product showed the presence of a majority phase identified with hydroxyapatite and a minority phase identified with tricalcium phosphate β. Thermal DTA / TGA measurements revealed three thermal mass loss intervals. These mass losses have been attributed to the dehydration of water, the decomposition of carbonates and the destruction of organic matter. At 1200°C about 31.60% of the total mass loss was observed... The adsorption of methylene blue on the synthesized products annealed at 105°C and calcined at 1200°C gave low removal yields at room temperature. However, the yield with non-calcined materials is greater than that of calcined materials. These low adsorption rates can be explained by the poor structuring of synthesized products, the presence of impurities in the materials and the formation of aggregates during the adsorption study. However, the uses of titanium dioxide as the main support of the synthesized apatite have contributed to increase the phenomenon of adsorption of the latter by synergistic effect and have further allowed easy separation of the mixture from the solution at the end of the adsorption.

ACKNOWLEDGEMENT

COMPETING INTERESTS

Authors have declared that no competing interests exist.

REFERENCES

1. Roudié P. Une richesse nationale africaine Les phosphates du Togo. Cahiers d'outre-mer. 1977;30(119):313–318. French.
   DOI: 10.3406/caoum.1977.2830.
2. Agbossoumonde DY. Les problèmes liés à l'extraction des ressources naturelles au Togo : Le cas des phosphates de hahotoé-kpogamé et des calcaires de Tabligbo au Sud Togo. 2011;10. French.
3. Rajan SSS, Watkinson JH, Sinclair AG. Phosphate rocks for direct application to soils. 1996;57:77–159.
   DOI: 10.1016/S0065-2113(08)60923-2.
4. UE. La commission européenne propose d'interdire les phosphates dans les détergents textiles, Bruxelle. 2010. French.
5. A. Corami, S. Mignardi, V. Ferrini. Copper and zinc decontamination from single- and binary-metal solutions using hydroxyapatite. Journal of Hazardous Materials. 2007;146 (1–2):164–170.
   DOI: 10.1016/j.jhazmat.2006.12.003.
6. Ramesh ST, Rameshbabu N, Gandhimathi R, Srikanth Kumar M, Nidheesh PV. Adsorptive removal of Pb(II) from aqueous solution using nano-sized hydroxyapatite. Applied Water Science. 2013;3(1):105–113.
   DOI: 10.1007/s13201-012-0064-z.
7. Saber-Samandari S, Saber-Samandari S, Gazi M. Cellulose-graft-polyacrylamide/ hydroxyapatite composite hydrogel with possible application in removal of Cu (II) ions. Reactive and Functional Polymers. 2013;73(11):1523–1530.
   DOI:10.1016/j.reactfunctpolym.2013. 07.007.
8. Seaman JC, Meehan T, Bertsch PM. Immobilization of Cesium-137 and Uranium in contaminated sediments using Soil Amendments. Journal of Environment Quality. 2001;30(4):1206.
   DOI: 10.2134/jeq2001.3041206x.
9. Shelobolina ES, Konishi H, Xu H, Roden EE. U(VI) Sequestration in hydroxyapatite produced by microbial glycerol 3-phosphate metabolism. Applied and Environmental Microbiology. 2009;75(18): 5773–5778.
   DOI: 10.1128/AEM.00628-09.
10. Fuller CC, Piana MJ, Bargar JR, Davis JA, Kohler M. Evaluation of apatite materials for use in permeable reactive barriers for the remediation of uranium-contaminated groundwater, in: Handbook of groundwater remediation using permeable reactive barriers, Elsevier. 2003;255–280.
11. Srilakshmi C, Saraf R. Ag-doped hydroxyapatite as efficient adsorbent for removal of Congo red dye from aqueous solution: Synthesis, kinetic and equilibrium adsorption isotherm analysis. Microporous and Mesoporous Materials. 2016;219: 134–144.
   DOI: 10.1016/j.micromeso.2015.08.003.
12. Jensen JE. Binding of dyes to chlorhexidine-treated hydroxyapatite. European Journal of Oral Sciences. 1977; 85(5):334–340.
   DOI: 10.1111/j.1600-0722.1977.tb01512.x.
13. Paul W, Sharma CP. Development of porous spherical hydroxyapatite granules: Application towards protein delivery. Journal of Material Science: Materials in Medecine. 1999;10:383–388.
14. Saber-Samandari S, Saber-Samandari S, Nezafati N, Yahya K. Efficient removal of lead (II) ions and methylene blue from aqueous solution using chitosan/Fe-hydroxyapatite nanocomposite beads. Journal of Environmental Management. 2014;146:481–490.
   DOI: 10.1016/j.jenvman.2014.08.010.
15. Safavi A, Momeni S. Highly efficient degradation of azo dyes by palladium/hydroxyapatite/Fe3O4 nanocatalyst. Journal of Hazardous Materials. 2012;201–202:125–131.
   DOI: 10.1016/j.jhazmat.2011.11.048.
16. Suen RB, Lin SC, Hsu WH. Hydroxyapatite-based immobilized metal affinity adsorbents for protein purification. Journal of Chromatography A. 2004;1048 (1):31–39.

DOI: 10.1016/j.chroma.2004.06.132.

17. Lemlikchi W, Drouiche N, Belaicha N, Oubagha N, Baaziz B, Mecherri MO. Kinetic study of the adsorption of textile dyes on synthetic hydroxyapatite in aqueous solution. Journal of Industrial and Engineering Chemistry. 2015;32:233–237.
    DOI: 10.1016/j.jiec.2015.08.023.

18. Seisuke K, Atsushi Y, Ryohei O, Masataka O, Masaru A, Hideki A. Application of Hydroxyapatite-sol as drug carrier. io-medical materials and engineering. 1994; (4):283–290.
    DOI: 10.3233/BME-1994-4404.

19. Jungbauer A, Hahn R, Deinhofer K, Luo P. Performance and characterization of a nanophased porous hydroxyapatite for protein chromatography. Biotechnology and Bioengineering. 2004;87(3):364–375.
    DOI: 10.1002/bit.20121.

20. Akpan UG, Hameed BH. Parameters affecting the photocatalytic degradation of dyes using TiO2-based photocatalysts: A review. Journal of Hazardous Materials. 2009;170(2–3):520–529.
    DOI: 10.1016/j.jhazmat.2009.05.039.

21. Kanna M, Wongnawa S. Mixed amorphous and nanocrystalline TiO2 powders prepared by sol–gel method: Characterization and photocatalytic study. Materials Chemistry and Physics. 2008; 110(1):166–175.
    DOI: 10.1016/j.matchemphys.2008.01.037.

22. Sanae EA. Nouveaux matériaux de structure apatite préparés à partir du phosphate naturel marocain à applications environnementales, MOHAMMED V – AGDAL; 2009.

23. El Asri S, Laghzizil A, Saoiabi A, Alaoui A, K. El Abassi, M'hamdi R, Coradin T. A novel process for the fabrication of nanoporous apatites from Moroccan phosphate rock.Physicochemical and Engineering Aspects. 2009;350(1–3):73–78.
    DOI: 10.1016/j.colsurfa.2009.09.006.

24. Perdikatsis B. X-ray powder diffraction study of francolite by the rietveld method. Materials Science Forum. 1991;79–82: 809–814.
    DOI:10.4028/www.scientific.net/MSF.79-82.809.

25. Zheng W, Li X, Yang Q, Zeng G, Shen X, Zhang Y, Liu J. Adsorption of Cd(II) and Cu(II) from aqueous solution by carbonate hydroxylapatite derived from eggshell waste. Journal of Hazardous Materials. 2007;147(1–2):534–539.
    DOI: 10.1016/j.jhazmat.2007.01.048.

26. Islam M, Chandra Mishra P, Patel R. Physicochemical characterization of hydroxyapatite and its application towards removal of nitrate from water. Journal of Environmental Management. 2010;91(9): 1883–1891.
    DOI: 10.1016/j.jenvman.2010.04.013.

27. Moustafa YM, El-Egili K. Infrared spectra of sodium phosphate glasses.Journal of Non-Crystalline Solids. 1998;240(1–3): 144–153.
    DOI: 10.1016/S0022-3093(98)00711-X.

28. Wei M, Evans JH, Bostrom T, Gréndahl L. Synthesis and characterization of hydroxyapatite, fluoride-substituted hydroxyapatite and fluorapatite. Journals of Materials Sciences: Materials in Medecine. 2003;14:10.

29. Fowler BO. Infrared studies of apatites I vibrational assignments for calcium, strontium, and barium hydroxyapatites utilizing isotopic substitution. Inorganic Chemistry. 1974;13(1):194–207.
    DOI: 10.1021/ic50131a039.

30. Rehman I, Bonfield W. Characterization of hydroxyapatite and carbonated apatite by photo acoustic FTIR spectroscopy. Journal of Materials Science: Materials in Medicine. 1997;8(1):1–4.
    DOI: 10.1023/A:1018570213546.

31. Manjubala I, Sivakumar M, Nikkath SN. Synthesis and characterisation of hydroxy/fluoroapatite solid solution. Journal of Materials Science. 2001;5481–5486.

32. Barka N, Qourzal S, Assabbane A, Nounah A, Aît-Ichou Y. Adsorption of disperse blue SBL dye by SYNTHESIZED poorly crystalline hydroxyapatite. Journal of Environmental Sciences. 2008;20(10): 1268–1272.
    DOI: 10.1016/S1001-0742(08)62220-2.

33. Pratap Reddy M, Venugopal A, Subrahmanyam M. Hydroxyapatite-supported Ag–TiO2 as Escherichia coli disinfection photocatalyst. Water Research. 2007;41(2):379–386.
    DOI: 10.1016/j.watres.2006.09.018.

34. Piccirillo C, Denis CJ, Pullar RC, Binions R, Parkin IP, Darr JA, Castro PML. Aerosol assisted chemical vapour deposition of hydroxyapatite-embedded titanium dioxide composite thin films. J Journal of

Photochemistry and Photobiology A: Chemistry. 2017;332:45–53.
DOI: 10.1016/j.jphotochem.2016.08.010.

35. Ozeki K, Janurudin JM, Aoki H, Fukui Y. Photocatalytic hydroxyapatite/titanium dioxide multilayer thin film deposited onto glass using an rf magnetron sputtering technique. Applied Surface Science. 2007; 253(7):3397–3401.
DOI: 10.1016/j.apsusc.2006.07.030.

36. Wold A. Photocatalytic properties of titanium dioxide (TiO2).

Chemistry of Materials. 1993;5(3):280–283.
DOI: 10.1021/cm00027a008.

37. Awazu K, Fujimaki M, Rockstuhl C, Tominaga J, Murakami H, Ohki Y, Yoshida N, Watanabe T. A plasmonic photocatalyst consisting of silver nanoparticles embedded in titanium dioxide. Journal of the American Chemical Society. 2008;130 (5):1676–1680.
DOI: 10.1021/ja076503n.